Robotics and Computer-Integrated Manufacturing 28 (2012) 57–65

Contents lists available at ScienceDirect

Robotics and Computer-Integrated Manufacturing

journal homepage: www.elsevier.com/locate/rcim

A novel XY-Theta precision table and a geometric procedure for its kinematic calibration

Ahmed Joubair, Mohamed Slamani, Ilian A. Bonev *

École de Technologie Supérieure, 1100, Notre-Dame Street West, Montreal, QC, Canada H3C 1K3

ARTICLE INFO

Article history:
Received 20 December 2010
Received in revised form
17 June 2011
Accepted 20 June 2011
Available online 20 July 2011

Keywords:
Parallel robot
Calibration
Accuracy assessment
Repeatability

ABSTRACT

Spatial precision positioning devices are often based on parallel robots, but when it comes to planar positioning, the well-known serial architecture is virtually the only solution available to industry. Problems with parallel robots are that most are coupled, more difficult to control than serial robots, and have a small workspace. In this paper, new parallel robot is proposed, which can deliver accurate movements, is partially decoupled and has a relatively large workspace. The novelty of this parallel robot lies in its ability to achieve the decoupled state by employing legs of a different kinematic structure. The robot repeatability is evaluated using a CMM and so are the actual lead errors of its actuators. A simple geometric method is proposed for directly identifying the actual base and mobile reference frames, two actuator's offsets and one distance parameter, using a measurement arm from FARO Technologies. While this method is certainly not the most efficient one, it yields a satisfactory improvement of the robot accuracy without the need for any background in robot calibration. An experimental validation shows that the position accuracy achieved after calibration is better than 0.339 mm within a workspace of approximately 150 mm × 200 mm.

1. Introduction

Parallel robots are often said to be more precise than serial robots because they do not suffer from error accumulation. While this might be true in theory [1], the real reason is that parallel robots can be built to be stiffer without being bulkier.

Spatial precision positioning devices are often based on hexapods (e.g., those manufactured by PI and ALIO Industries) or tripods (e.g., the SpaceFAB manufactured by MICOS). However, when it comes to planar three-degree-of-freedom (3-DOF) positioning, virtually all commercial so-called *XY-Theta positioning tables* are based on the well-known sandwich setup illustrated in Fig. 1. This serial configuration has the advantage of simple motion control. However, being "serial" means that the first actuator has to support the weight of all the other actuators. As a result, the device would have to be large enough not only to support itself, but to absorb any vibrations caused by the motors. This means that such a device would be relatively large and sluggish as well.

Planar parallel robots have received considerable attention (see [2] and the references therein), yet very few of them are used in industry. Most precision positioning prototypes based on planar parallel robots rely on the use of flexures (e.g., [3,4]). Yet, such robots have a very limited workspace-to-footprint ratio, and are not an alternative to the XY-Theta stage in Fig. 1.

Among the few existing planar 3-DOF parallel robot prototypes that do not employ flexures, one is based on a symmetric 3-*PRP*[1] architecture [5], where the base actuators form an equilateral triangle and the platform linear guides form a star. This robot has a very limited workspace though. In contrast, the 3-*RRP* robot first disclosed in [6], then studied in [7], and of which a first prototype was reported in [8], offers unlimited rotation in addition to excellent stiffness in the vertical direction. However, the achievable accuracy of such a robot is questionable, since it relies on the use of a perfectly circular rail.

The only commercially available parallel XY-Theta positioning table, manufactured by Hephaist Seiko and at least two other Japanese companies, is the one shown in Fig. 2. This robot is also based on the 3-*PRP* architecture, but its design is asymmetric. The resulting positioning table is very rigid, since its mobile platform glides directly on top of three linear guides. Unfortunately, this design is highly coupled, meaning that to move in certain directions all three actuators must work in conjunction with one another. Furthermore, its workspace is severely limited, as illustrated in [9].

* Corresponding author. Tel.: +1 514 396 8403.
E-mail address: ilian.bonev@etsmtl.ca (I.A. Bonev).

[1] It is customary to refer to parallel robots using the symbols *P* and *R*, which stand for prismatic and revolute joints, respectively. When a joint is actuated, its symbol is underlined.

0736-5845/$ - see front matter © 2011 Elsevier Ltd. All rights reserved.
doi:10.1016/j.rcim.2011.06.006

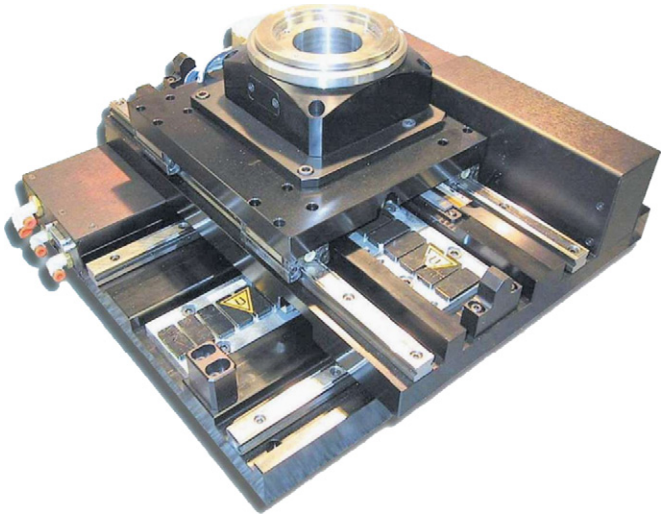

Fig. 1. A serial XY-Theta positioning table (courtesy of Newport Corp.).

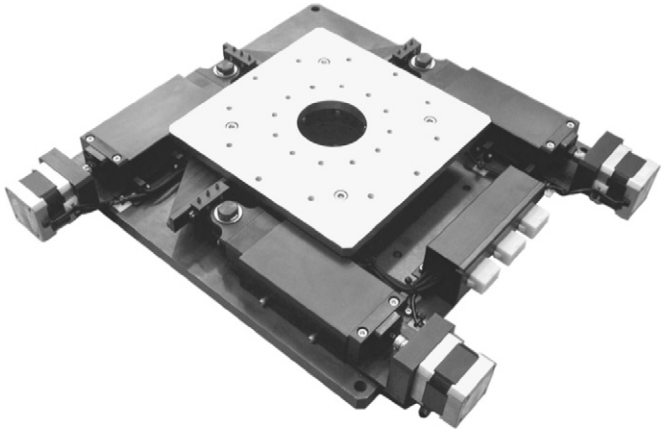

Fig. 2. NAF3 alignment stage (courtesy of Hephaist Seiko Co., Ltd.).

This paper presents for the first time the prototype of a novel patented XY-Theta parallel architecture [10], dubbed the PreXYT, that is both partially decoupled, rigid in all directions, and having a relatively large workspace, and proposes a geometric procedure for the kinematic calibration of the robot. In particular, Section 2 briefly recalls from [9] the kinematic analyses of the PreXYT, but in a slightly more general fashion. Section 3 discusses the actual prototype and Section 4 presents the results on the repeatability of that prototype, as assessed using a CMM (a Coordinate Measuring Machine). Section 5 briefly presents the identification of the lead errors for all three actuators, using the same CMM. Section 6 describes the proposed calibration procedure based on the use of a measurement arm and Section 7 presents the results on the improved accuracy. Finally, conclusions are provided in Section 8.

2. Kinematic analyses

2.1. Direct and inverse kinematic analysis

PreXYT is a parallel robot with one *PPR* leg and two *PRP* legs, as shown in Fig. 3. The directions of the actuators in legs 2 and 3 are parallel to the y axis of a base reference frame, while the direction of the actuator in leg 1 is parallel to the x axis. The two passive prismatic joints on the mobile platform are parallel and the axes of the three revolute joints are parallel and coplanar.

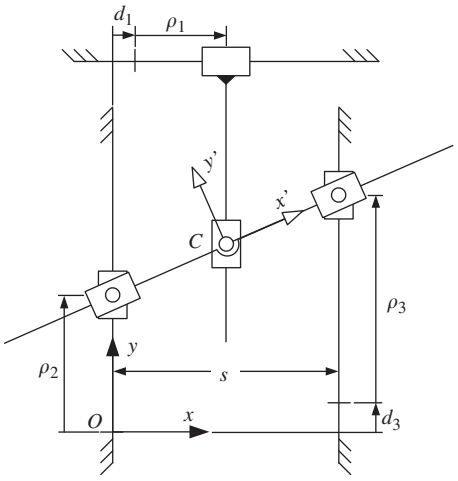

Fig. 3. Schematic diagram of the PreXYT.

The directions of the two prismatic joints in leg 1 are normal. Consequently, if the two parallel actuators move in conjunction with one another at the same rate, the mobile platform is only translated along the y axis. If the two move in opposite directions, a pure rotation about the z axis could occur. Finally, the other actuator directly controls the x coordinate of the platform's center.

Referring to Fig. 3, the base reference frame Oxy is fixed at the base so that the axis of the revolute joint of leg 2 always intersects the y axis, and a mobile reference frame $Cx'y'$ is fixed to the mobile platform so that the axes of the revolute joints of legs 2 and 3 always intersect the x' axis. The origin C lies on the axis of the revolute joint of leg 1. Finally, θ is the angle between the x and x' axes, measured counterclockwise.

Furthermore, ρ_1 is the active-joint variable associated with leg 1 and is defined as the distance between the y axis and (the axis of) the revolute joint of leg 1 minus an offset d_1 as illustrated in Fig. 3. Similarly, ρ_3 is the active-joint variable associated with leg 3 and is defined as the distance between the x axis and the revolute joint of leg 3 minus an offset d_3. The active-joint variable ρ_2 is defined as the distance between the x axis and the revolute joint of leg 2, i.e., the offset $d_1=0$. These offsets represent the relative positions of the mechanical limit switches. Finally, s is the distance between the y axis and the axis of the revolute joint of leg 3.

Given the active-joint variables, we are able to uniquely define the position and orientation of the mobile platform (i.e., of the mobile reference frame). The orientation angle is easily obtained as

$$\theta = \tan^{-1}\left(\frac{\rho_3+d_3-\rho_2}{s}\right), \tag{1}$$

While the position of the mobile platform is given by

$$x = \rho_1+d_1, \tag{2}$$

$$y = \rho_2+(\rho_1+d_1)\left(\frac{\rho_3+d_3-\rho_2}{s}\right). \tag{3}$$

As can be observed, the direct kinematic equations of the PreXYT are relatively simple, and the platform's x coordinate is directly defined by actuator 1, which is why our parallel robot is partially decoupled.

The inverse kinematics are also simple. Given the position and orientation of the platform, the active-joint variables are defined by

$$\rho_1 = x-d_1, \tag{4}$$

$$\rho_2 = y-x\tan\theta, \tag{5}$$

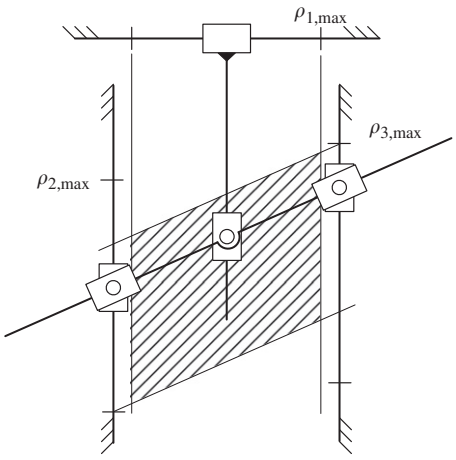

Fig. 4. Constant-orientation workspace of the PreXYT.

$$\rho_3 = y + (s-x)\tan\theta - d_3. \quad (6)$$

Finally, it is evident that the PreXYT has no singularities whatsoever.

2.2. Workspace analysis

The so-called *constant-orientation workspace* is the set of positions attainable by the platform's center C for a fixed orientation of the platform, given the actuator limits ($\rho_{1,max}$, $\rho_{2,max}$, $\rho_{3,max}$), as illustrated in Fig. 4, where the constant-orientation workspace for a given orientation is the hatched region. The constant-orientation workspace of the PreXYT is delimited by two lines parallel to the x axis and passing through the limits of actuators 2 and 3, and by two lines parallel to the y axis and passing through the limits of actuator 1. Obviously, the greater the orientation, the smaller is the constant-orientation workspace.

A more meaningful workspace subset would be the set of positions attainable by the platform's center C with all possible orientations within a given interval $[-\theta_m, \theta_m,]$. In the PreXYT, this workspace has a hexagonal form and can be easily computed by finding the intersection of the constant-orientation workspaces at $-\theta_m$ and at θ_m.

3. Prototype

A prototype of the PreXYT, shown in Fig. 5, has been constructed at the École de technologie supérieure. It comprises three screw-driven linear guides from LinTech: two from the 130 series and one from the 100 series. Each of the two 130 series linear guides has a pivoting block attached to the carriage through a deep-groove single-row bearing. A steel shaft is rigidly attached to one of the two pivoting blocks and, through a simple linear ball bearing, to the other pivoting block. This important modification from the original design in Fig. 3, while having no impact on the kinematic model of the PreXYT, is not only simpler to implement, but also eliminates the presence of a reciprocating rod at one side of the robot, which leads to a more compact device. The mobile platform slides along the rod through a pair of the same linear ball bearings. The carriage of a roller monorail guide is attached to the carriage of the LinTech 100 series linear guide, so that the two guides are perpendicular. The monorail guide is fixed to the tapered block, which holds a large deep-groove double-row ball bearing that is attached to the mobile platform.

The LinTech 100 series linear guide has a wider carriage and a much higher loading capacity (a 576 Nm roll moment, compared to 38 Nm for the 130 series), minimizing the deflection that would occur when the mobile platform is at the extreme ends of the monorail guide (the passive prismatic joint in leg 1). Overall, this mechanical design provides high rigidity in all directions, and particularly in the z direction, which yields a large payload capacity.

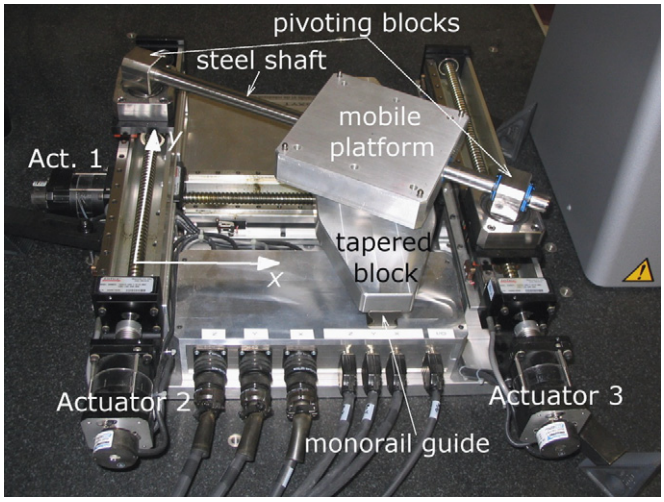

Fig. 5. Experimental setup for measuring the repeatability of the PreXYT with a CMM.

The 100 series and the two 130 series linear guides have travel lengths limited through mechanical limit switches to about 170 and 300 mm, respectively. The distance s (Fig. 3) is about 394 mm. As a result, the mobile platform can rotate up to $\pm 35^\circ$ and translate inside a rectangle 170 mm × 300 mm, when at 0°. Or, referring to the more practical workspace subset defined in the previous section, the set of positions attainable with any orientation between -17° and 17° is at least a disk of diameter 170 mm. For comparison, the mobile platform is about 160 mm × 160 mm and the base plate is 470 mm × 510 mm.

The motors of the linear guides are CMC BNL 2310 brushless servo motors, yielding a maximum continuous torque of less than 0.7 Nm. No gear boxes are used, since the linear guides use Acme precision ball screws of 5.080 mm (0.2 in) lead, with a specified maximum lead error of 50 μm per 300 mm, zero backlash, and bidirectional repeatability of 5 μm.

We use no linear absolute encoders but only incremental encoders integrated into the motors. Their resolution is 8000 pulses per revolution, which translates to about 0.6 μm of linear resolution. Obviously, this is more than sufficient, since the repeatability of the linear guides is 5 μm. Furthermore, when homing each actuator, we use both the mechanical limit switch and the index pulse.

Finally, we used an AMP-20540 four-axis drive module and a DMC-2133 four-axis controller from Galil. We interfaced these with a UniOp HMI device with a touch screen and put all these components in the table top rack cabinet (not shown in Fig. 5).

The cost of the off-the-shelf components was about $15,000. The cost of machining, assembly, cabling, and programming, all carried out in-house, cannot be estimated.

4. Assessment of the position repeatability

We were concerned that average repeatability would be compromised as a result of using relatively low-cost components. Nevertheless, we performed all measurements using the best equipment available, at a constant temperature of 24 °C, fixing

four tooling balls at the corners of the mobile platform (but using only one). There are no data on the sphericity of these balls, but their manufacturer specifies a diameter of 6.35 mm ± 5 μm (0.25 ± 0.0002 in.). We used a Mitutoyo Bright-STRATO 7106 CMM, as shown in Fig. 5. Its recent certificate indicates a total measurement uncertainty of 2.7 μm at 2σ. Furthermore, we tested the repeatability of the CMM by measuring three of the tooling balls on the (stationary) mobile platform thirty times. The worst repeatability, calculated using Eqs. (7–10), was better than 1.4 μm (at 3σ).

There is no standard procedure for measuring the repeatability of a parallel robot. The best procedure will be the one that reveals the worst repeatability. In [12,13], the authors used laser interferometers to measure the positioning error of their parallel kinematic machines according to the procedures outlined in the machine tool performance testing standards [14]. However, since our device will rather be used as a robot, we decided to use the following procedure, inspired by the ISO 9283 norm [15] (for industrial robots), which consists of a trajectory connecting five measurement poses (P_1, P_2, …, P_5) and repeated 30 times, as illustrated in Fig. 6. This procedure induces a hysteresis effect at measurement pose P_1.

Pose repeatability expresses the closeness of agreement between the poses attained after n repeat visits to the same *command pose* [15]. Our procedure will measure both *unidirectional repeatability* (at P_2, P_3, P_4, and P_5,) and *multidirectional repeatability* (at P_1). Finally, since we measure the coordinates of only one point from the mobile platform (the center of a tooling ball), we actually evaluate *position repeatability* and not pose repeatability. Also, the orientation of the mobile platform is kept at 0°, all displacements are made at a constant speed of 0.4 m/s, and there is no payload. We performed similar tests at different orientations of the mobile platform, and we also measured the orientation repeatability at several positions. However, the analyses of the results from these measurements did not reveal any further insights and will not be presented in this paper.

There are two approaches for evaluating position repeatability, ε, from a set of n points. The most natural one is to find the radius of the smallest sphere (or, in the planar case, circle) that encloses all points. The other measure for evaluating position repeatability is to calculate the mean position error with respect to the barycentre $(\bar{x},\bar{y},\bar{z})$ of the cluster of n points (x_i, y_i, z_i) and add three times the standard deviation [15]

$$\varepsilon = \bar{r} + 3\sigma_r, \tag{7}$$

where

$$\bar{r} = \frac{1}{n} r_i, \tag{8}$$

$$\sigma_r = \sqrt{\frac{\sum_{i=1}^{n} (r_i - \bar{r})^2}{n-1}}, \tag{9}$$

$$r_i = \sqrt{(x_i - \bar{x})^2 + (y_i - \bar{y})^2 + (z_i - \bar{z})^2}. \tag{10}$$

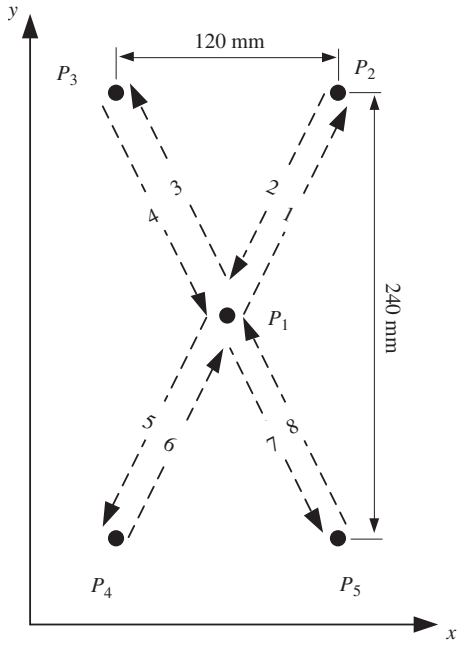

Fig. 6. Sequence for measuring position repeatability (not to scale).

Table 1 shows the final results. Note that, even though we have measured the position at P_1 120 times, we only consider the first 30 measurements. Considering all 120 measurements yields nearly identical results.

The first observation is that the worst repeatability, naturally occurring at P_1, is about 30 μm. For comparison, the bidirectional repeatability of an *xy* serial arrangement of two of our linear guides would be at least about 7 μm (since the bidirectional repeatability of our guides is 5 μm). Indeed, it is obvious that the repeatability of a parallel robot would be worse than that of an "equivalent" serial robot, since it is affected by the mechanical imperfections (backlash, elasticity, etc.) of many additional components, primarily passive joints.

A plot of all $\{x, y\}$ measurements at P_1 and P_2 is shown in Fig. 7 (the x and y coordinates in these figures are those of the tooling ball measured, and not of the platform's center). Note that the upper cluster of points in Fig. 7a corresponds to arrivals at P_1 from "above" (i.e., from P_2 and P_3), while the lower cluster of points corresponds to arrivals from "below" (i.e., from P_4 and P_5). Thus, there is an obvious hysteresis effect, which we believe is in large part due to clearances in the INA KX12 linear bearings through which the steel shaft reciprocates. These linear bearings allow axis misalignment of up to 40 arcmin, which translates to a clearance of about 24 μm (given their length of 41.27 mm). However, this clearance alone cannot be the reason why the repeatability at P_2 and P_3 is much worse than that at P_4 and P_5. Therefore, we believe that another error is responsible, which is the warping of the mechanism due to the non-coplanarity of the two parallel guides.

The position repeatability along the y axis is much worse than that along the x axis for all five measurement poses, despite the fact that the arrival direction at four of the poses is always the same, as seen in Fig. 7b, for P_2. The clearance in the INA KX12 linear bearings and the warping of the mechanism should be the reason once again. Indeed, the x positioning at the zero orientation is influenced almost exclusively by leg 1. Since both the passive linear guide and the bearing of leg 1 are very stiff, the x positioning is very repeatable.

Table 1
Positioning repeatability (in μm).

Meas. pose	Radius of minimum boundary sphere/circle		Mean position repeatability				
	x, y, z	*x, y*	*x, y, z*	*x, y*	*x*	*y*	*z*
P_1	28.8	27.1	32.4	30.4	7.3	30.1	11.3
P_2	12.3	12.1	15.5	15.2	2.7	15.2	5.0
P_3	8.5	8.3	11.4	11.3	2.9	11.4	4.5
P_4	3.2	3.0	4.4	4.2	2.1	4.0	2.7
P_5	4.9	4.9	6.2	6.0	2.3	6.2	3.1

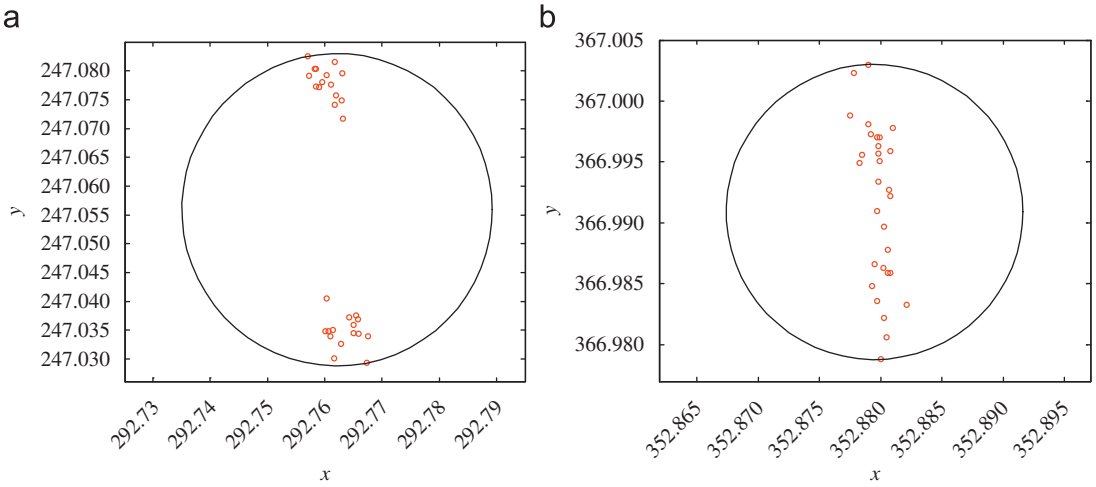

Fig. 7. Projections in the *xy* plane of the thirty position measurements at poses (*a*) P_1 and (*b*) P_2.

The mechanism does indeed undergo slight warping, which can be seen from analyzing the coplanarity of the positions in P_2, P_3, P_4, and P_5. If we take the centers of the bounding spheres for the measurements at these four poses, then we can calculate that the distance from any of these centers to the plane formed by the other three centers is 52 μm.

Finally, note that the measurements shown in Table 1 were performed after a single homing. However, we also tested the repeatability of our homing procedure by measuring the position of our tooling ball after ten successive homing sequences, at the home position. This repeatability is better than 2 μm (at 3σ).

5. Determination of lead errors

As already mentioned, the maximum lead error of our linear guides is 50 μm per 300 mm and we do not use absolute linear encoders. Therefore, to improve the accuracy of the PreXYT, we measured the actual lead error on the CMM using the following procedure. A precision ball of diameter 9.525 mm (3/8 in.) was solidly attached to the carriage of each of the three linear guides using magnetic nests and hot glue. The range of motion of each actuator was divided into six segments, i.e., seven consecutive positions at which measurements were taken. Each fist position corresponded to when the actuator is homed and was considered at the reference position. Each actuator is then moved to each of the subsequent six positions, and at each position the precision ball is measured using the CMM. The measurement sequence for each actuator is repeated ten times (i.e., measurements are done at positions $1\rightarrow2\rightarrow3\rightarrow4\rightarrow5\rightarrow6\rightarrow1\rightarrow2\ldots$). A linear regression is then applied for each actuator and the actual lead is determined. The actual screw errors were thus determined to be $-0.690\times10^{-3}\rho_1$, $-0.454\times10^{-3}\rho_2$, and $-0.358\times10^{-3}\rho_3$ (i.e., the actual lead for actuator 1 is 5.0764948 mm instead of 5.080 mm, etc.) or as much as 200 μm per 300 mm.

6. Kinematic calibration

While the repeatability of the PreXYT was assessed using a CMM and so were the actual lead errors, we decided to use our own FaroArm Platinum measurement arm for the robot calibration. This choice was made mainly because not only is our FaroArm accessible to us at all times and much easier to use, but also because the FaroArm has a volumetric accuracy that is sufficiently good for the calibration of the PreXYT. Indeed, the 3D point-to-point accuracy of our 4 ft FaroArm Platinum is specified at ±18 μm. Of course, unlike the CMM where triggering is automatic, the accuracy of measurements with the FaroArm is highly dependent on the experience of the operator and on the rigid mounting of the FaroArm.

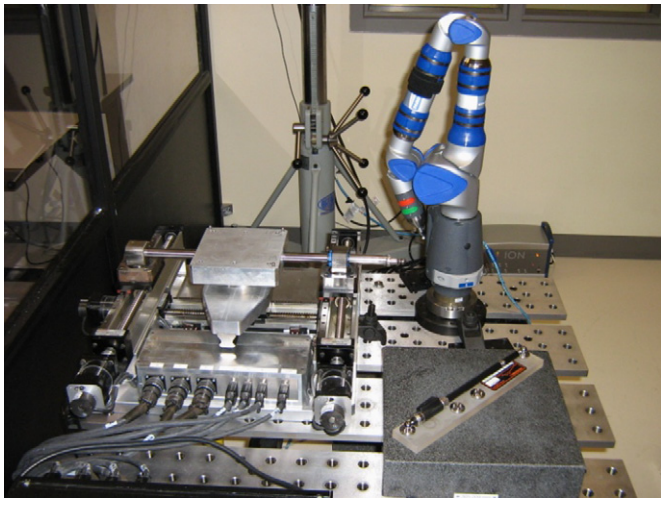

Fig. 8. Experimental setup for calibrating the PreXYT with a FaroArm.

Fig. 8 shows the setup used for calibrating the PreXYT and for assessing the point-to-point accuracy of the FaroArm. Both the PreXYT and the FaroArm are solidly attached to a heavy steel table. The FaroArm is equipped with its standard 3 mm probe and is used by probing the same tooling balls (attached to the mobile platform) described in Section 4 and the same precision balls described in Section 5.

We assessed the point-to-point accuracy of our FaroArm using a 300 mm scale bar (actually, the calibration kit of our Renishaw telescoping ballbar). The scale bar was positioned in two configurations: the one shown in Fig. 8 and another one obtained by rotating the bar at 90°. At each configuration, each of the two high precision balls of the scale bar was measured ten times using the PolyWorks software. In the scale-bar configuration shown in Fig. 8, the mean distance error was -6 μm and the standard deviation was 4 μm, while in the second configuration, the mean distance error was 12 μm and the standard deviation was 5 μm. We also measured ten times the center of one of the tooling balls

on the mobile platform (while the robot controller was turned off) and repeatability, calculated using Eqs. (7–10), was better than 7.3 μm (at 3σ). Therefore, we believe that the FaroArm can be used for calibrating the PreXYT, since the multidirectional repeatability of our robot is more than 30 μm and the volumetric accuracy that we aim at is certainly not less than 100 μm.

There exist two major families of calibration methods [16]: kinematic and non-kinematic. A kinematic calibration approach considers that the robot's links are perfectly rigid. Therefore, the calibration is to introduce corrections only to the kinematic model of the robot. On the other hand, a non-kinematic calibration takes into account that the robot is affected by some non-geometric errors, such as the elasticity of joints, the transmission errors of gears and their backlash, the effects of temperature [17] and speed. This calibration implies that the model of the robot must take into account various non-geometric parameters, which makes the model very complex, and renders the direct and inverse kinematics of the robot more difficult to solve.

Our work considers only a basic kinematic calibration although we also determine the lead errors. Several researches use this approach to calibrate parallel robots, by performing measurements on the actuators [18] or on the end-effector [19–22]. Both approaches are used to find the parameters that minimize the residuals of either the inverse or direct kinematic model. Some methods add mechanical constraints to the robot, to limit some of its movements during the calibration procedure. This can be achieved by blocking the position or orientation of the end-effector to a known value [23], or by forcing it to make a specific movement such as linear trajectory or to move along a predefined plan [24]. For more details about parallel robot calibration methods, the reader is referred to [25].

A calibration approach can use position data from the internal sensors of a robot [24] and, possibly, from an external 3D measurement device such as a CMM [26], a CCD camera [27,28], a laser tracker [17], or other 2D or even 1D measurement devices such as an inclinometer [29], a theodolite [30,31], a triad of dial gages [32] or a telescopic ballbar [33]. In most cases, the calibration is based on an optimization method that finds the parameters improving the robot's accuracy. While it is generally accepted that such approaches yield better results than when trying to directly measure the robot geometry (an approach known as screw-axis measurement in the case of serial robots [34]), there are virtually no reported works on such direct methods in the case of parallel robots. The only exceptions are references [35,36], both describing direct geometric methods for calibrating spatial parallel robots with cylindrical legs. In comparison to the present work, the first work [35] was too superficial, while the second work [36] used a single CCD camera. However, none of the methods proposed in these two works is directly applicable to the PreXYT.

In this paper, we will use a geometric approach for obtaining the actual robot kinematic parameters. Furthermore, we will determine only those kinematic parameters that do not render the kinematic equations of the PreXYT more coupled. In other words, we will determine only the base and mobile reference frames, the actuator offsets d_1 and d_3, and the distance s, and keep all other parameters at their nominal values. We already know that while the direction of actuator 1 is precisely orthogonal to the directions of actuators 2 and 3 (the assembly of the robot was done with the help of the CMM), the orthogonality between the directions of the two prismatic joints in leg 1 is relatively poor and there are certainly many other geometric errors that we neglect. However, in this paper, our aim is not to achieve the best robot accuracy possible, but to analyze the limits of directly measuring the main robot parameters only (thus keeping the kinematic model as simple as possible). The idea is to propose a method that can be understood and implemented by a technician with no expertise in robot calibration.

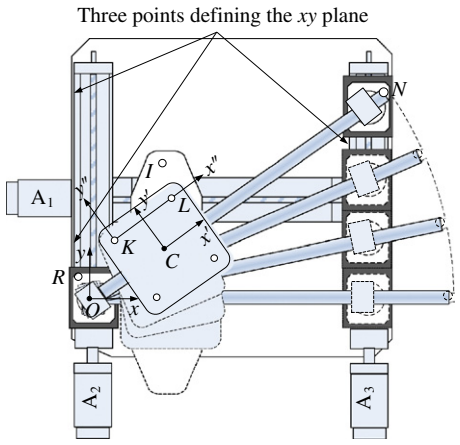

Fig. 9. Procedure for determining the base reference frame.

6.1. Determination of the base reference frame

The procedure for determining the base reference frame is illustrated in Fig. 9. Firstly, two points on the rail of actuator 2 and one point on the rail of actuator 3 are measured and used to define the xy plane of our robot. All further measurements will be projected in this plane. Next, the PreXYT is sent to its home position. A 3/8-in. precision ball, referred to as ball N, is attached at the free end of the steel shaft. Actuator 3 is then displaced in equal increments until the platform makes an angle of approximately 35°. At each increment, the position of (the center of) ball N is measured. A total of 36 positions are measured and they are supposed to lie on a 35° circular arc. The center of this arc, projected on the xy plane, gives us the origin O of the base reference frame.

We used the Gauss–Newton least-squares fitting method [37], to find the center of the circular arc. Of course, we are well aware of the fact that a 35° circular arc is not optimal for precisely determining the center of the circle. However, the maximum radius residual for the 36 positions was only 20 μm, and the norm of all residuals was 47 μm. Furthermore, since all other parameters are determined with respect to the base reference frame at this origin, this 35° limitation does not seem to be a major problem.

Next, we attach another 3/8-in. precision ball, referred to as ball R, on the carriage of actuator 2. We measure its position at the home position of actuator 2 and at its upper limit, some 300 mm farther away. The line that passes through both positions defines the direction of the base y axis. Finally, the x axis is orthogonal to the y axis, in the xy plane and pointing towards actuator 3.

6.2. Determination of mobile reference frame

The method for determining the origin C of the mobile reference frame is similar to the one for determining the origin O. We attach one precision ball, referred to as I, to the tapered block and use two of the four tooling balls attached to the platform, referred to as K and L, as shown in Fig. 9. As already mentioned in Section 3, the mobile platform is fixed to the tapered block through a large deep-groove double-row ball bearing. Thus, the origin C that we look for lies on the axis of rotation of this ball bearing. The procedure, therefore, involves sending the mobile platform in the center of the workspace and rotating it from −35° to 35° in increments of 2°. At each orientation, we measure the centers of balls K, L, and I, project them to the Oxy plane and transform the coordinates of I to a reference frame with origin at K and with its x''

axis passing through L (Fig. 9). The transformed coordinates of the 36 measurements of I are then fitted to a circle with the Gauss–Newton least-squares fitting method [37]. The maximum radius residual for the 36 positions was only 10 μm, and the norm of all residuals was 23 μm. With respect to the $Kx''y''$ reference frame, that position was found to be {−73.932 mm, 72.947 mm}, while the nominal position is {−73.000 mm, 73.000 mm}.

The next step should be defining the x' axis of the mobile reference frame. This was done by displacing in several increments only actuator 1 from the configuration shown in Fig. 9, and measuring the positions of balls K and L. It was found out that balls K and L follow nearly the same path. Therefore, for simplicity, we neglected the slight offset and defined axis x' to be parallel to axis x''.

6.3. Determination of the distance s

Fig. 10 illustrates the idea behind the method used for determining the distance s (Fig. 3). The PreXYT is brought to the one of the configurations shown in Fig. 10 and then to the other by only displacing actuator 2. In each configuration, the steel shaft is probed and the measurements fitted to a cylinder, the axis of which is projected to the Oxy plane (all done in PolyWorks V13). The parameter s is the distance between the Oy axis and the point of intersection of the two projected axes. Note that the steel shaft (INA WZ3/4) is specified to have a diameter of 19.050 mm (3/4 in.), a parallelism of 9 μm, and a roundness of 6 μm. The procedure was repeated several times, and the mean value for the distance s was found to be 393.517 mm (with a standard deviation of 9 μm), while the nominal value is 394.000 mm.

6.4. Determination of the offsets d_1 and d_3

Fig. 11 illustrates the method used for determining the offsets d_1 and d_3. We home the PreXYT, and from its home configuration, we displace actuators 2 and 3 exactly 150 mm (half their range). This is done in order to eliminate the effect of the error in the orthogonality between the two prismatic joints in leg 1. Then, we measure the positions of balls K and L in order to obtain the position of C with respect to the base reference frame Oxy. The x coordinate of the position of C is the offset d_1. Next, we displace actuator 1 to the end of its range and measure the coordinates of ball K. Let the relative displacement of the center of ball K with respect to the base reference frame Oxy be denoted by $\{\Delta x, \Delta y\}$.

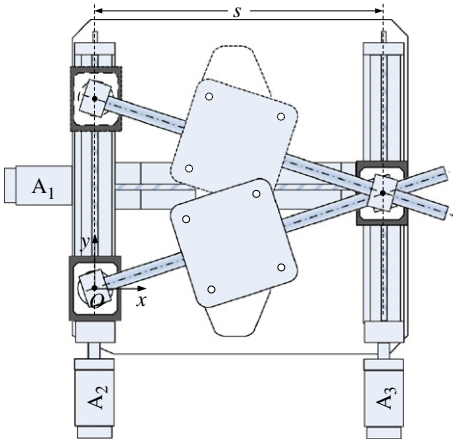

Fig. 10. Procedure for determining the distance s.

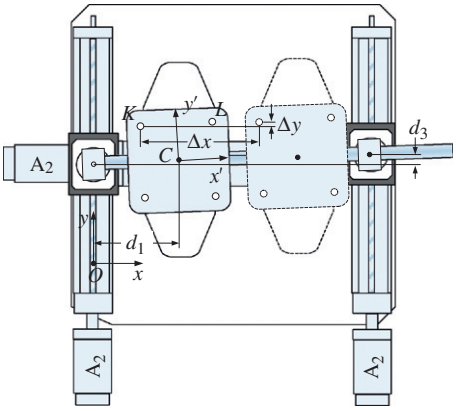

Fig. 11. Procedure for determining the offsets d_1 and d_3.

Then the offset d_3 is defined by the following formula:

$$d_3 = s\frac{\Delta y}{\Delta x}. \tag{11}$$

The above procedure was repeated several times (each time homing the robot) and the average values obtained were d_1 = 116.007 mm (with a standard deviation of 2 μm) and d_3 = 0.704 mm (with a standard deviation of 4 μm). The nominal values were d_1 = 115.000 mm and d_3 = 0.000 mm.

7. Experimental validation

To validate the efficiency of our calibration method, we performed measurements at five positions (the corners of a rectangle and its center [15]) for two different orientations, as well as for the central position and a range of orientations. We performed the same measurements, before calibration (using the nominal screw leads and the nominal values for the position of the origin C and for s, d_1 and d_3) and after calibration (using the new values for the screw leads, for the position of the origin C, and for s, d_1 and d_3). Of course, we first defined the base reference frame using the procedure described in Section 6.1, and used the same base frame for all measurements. Finally, all measurements were done with the FaroArm, in the same setup used for the calibration of the PreXYT and shown in Fig. 8, by measuring the centers of tooling balls K and L (and thus determining the coordinate of the platform center C). The whole procedure was repeated five times and the errors shown in this section are the mean values. Because of lack of space, the standard deviation for each measured position is not given, but even the worst one was only 13 μm.

The results are shown in Tables 2–4. In summary, the maximum position and orientation errors before calibration were 1.514 mm and 0.131°, respectively. The maximum position and orientation errors after calibration were reduced to 0.339 mm and 0.037°, respectively.

8. Conclusions

Despite the low-cost off-the-shelf components, we were able to build a first prototype of a novel 3-DOF planar parallel robot, dubbed PreXYT, with good positioning repeatability and pose accuracy. Videos of the PreXYT are available at http://www.youtube.com/CoRoETS.

We also proposed a calibration method that is simple to understand and perform, and that relies on the same trivial kinematic model as the nominal one. It was clearly demonstrated

Table 2
Pose accuracy at the orientation $\theta=0^\circ$.

Command position (in mm)	Mean position errors (in mm) and mean orientation errors (in degrees)							
	Before calibration				After calibration			
	x	y	x, y	θ	x	y	x, y	θ
{201.000, 137.500}	1.013	0.468	1.116	0.125	−0.017	0.238	0.238	0.022
{276.000, 250.000}	1.134	0.573	1.271	0.130	0.155	0.254	0.297	0.023
{126.000, 250.000}	1.247	0.355	1.296	0.125	0.159	0.299	0.339	0.020
{126.000, 25.000}	0.893	0.390	0.975	0.129	−0.193	0.241	0.309	0.030
{276.000, 25.000}	0.776	0.625	0.996	0.131	−0.208	0.231	0.311	0.031

Table 3
Pose accuracy at the orientation $\theta=10^\circ$.

Command position (in mm)	Mean position errors (in mm) and mean orientation errors (in degrees)							
	Before calibration				After calibration			
	x	y	x, y	θ	x	y	x, y	θ
{201.000, 137.500}	1.011	0.679	1.218	0.120	−0.023	0.239	0.240	0.013
{266.000, 220.000}	1.093	0.807	1.359	0.123	0.102	0.256	0.275	0.013
{136.000, 220.000}	1.189	0.630	1.346	0.117	0.099	0.305	0.321	0.010
{136.000, 55.000}	0.946	0.611	1.126	0.127	−0.154	0.237	0.282	0.021
{266.000, 55.000}	0.834	0.791	1.150	0.128	−0.160	0.193	0.251	0.021

Table 4
Pose accuracy at the position {201.000 mm, 137.500 mm}.

Command orientation (degrees)	Mean position errors (in mm) and mean orientation errors (in degrees)							
	Before calibration				After calibration			
	x	y	x, y	θ	x	y	x, y	θ
−29	1.020	−0.263	1.054	0.099	0.021	0.224	0.225	0.037
−19	1.022	−0.001	1.022	0.113	0.012	0.223	0.224	0.036
−9	1.024	0.243	1.052	0.126	−0.003	0.229	0.229	0.031
0	1.022	0.452	1.117	0.129	−0.014	0.234	0.234	0.023
9	1.017	0.653	1.208	0.124	−0.024	0.234	0.235	0.015
19	1.011	0.876	1.338	0.113	−0.032	0.227	0.229	0.006
29	1.004	1.134	1.514	0.100	−0.044	0.221	0.225	−0.002

that such a calibration method can lead to greatly improving the accuracy of the robot (by a factor of almost five). To further improve the accuracy of the robot, we need to identify additional design parameters, the most important being the angle between the two passive joints in leg 1. While this could have been easily done using our geometric approach, taking this error into consideration would have inevitably led to more complex kinematic equations, which is why we deliberately ignored it.

Acknowledgments

We would like to thank the Fonds québécois de la recherche sur la nature et les technologies (FQRNT) and the Canada Research Chair program for financially supporting this work.

References

[1] Briot S, Bonev IA. Are parallel robots more accurate than serial robots. Transactions of the Canadian Society for Mechanical Engineering 2007;31(4):445–55.
[2] Bonev IA, Zlatanov D, Gosselin CM. Singularity analysis of 3-DOF planar parallel mechanisms via screw theory. Journal of Mechanical Design 2003;125(3):573–81.
[3] Hesselbach J, Wrege J, Raatz A, Becker O. Aspects on design of high precision parallel robots. Assembly Automation 2004;24(1):49–57.
[4] Zhang Z, Mills JK, Cleghorn WL. Multi-mode vibration control and position error analysis of parallel manipulator with multiple flexible links. Transactions of the Canadian Society for Mechanical Engineering 2010;34(2):197–213.
[5] Ronchi S, Company O, Pierrot F, Fournier A. PRP planar parallel mechanism in configurations improving displacement resolution. In: Proceedings of the 1st international conference on positioning technology, Act-city, Hamamatsu, Japan, June 9–11; 2004.
[6] Scheidegger A, Liechti R. Positioning device. US Patent No. 6,622,586, filed on December 21, 2001, issued on September 23, 2003.
[7] Bonev IA, Yu A, Zsombor-Murray P. XY-Theta positioning table with parallel kinematics and unlimited Theta rotation. In: Proceedings of the IEEE international symposium on industrial electronics, Montreal, QC, Canada, July 9–13; 2006.
[8] Lotfi B, Zhong ZW, Khoo LP. A novel algorithm to generate backlash-free motions. Mechanism and Machine Theory 2010;45(8):1171–84.
[9] Yu A, Bonev IA, and Zsombor-Murray P. New XY-Theta positioning table with partially decoupled parallel kinematics. In: Proceedings of the IEEE International Symposium on Industrial Electronics, Montreal, QC, Canada, July 9–13; 2006.
[10] Bonev IA. Planar parallel mechanism and method. US Patent No. 7,707,907, filed November 17, 2006, issued May 4, 2010.
[12] Wang L, Wu J, Wang J, You Z. An experimental study of a redundantly actuated parallel manipulator for a 5-DOF hybrid machine tool. IEEE/ASME Transactions on Mechatronics 2009;14(1):72–81.
[13] Dong J, Yuan C, Stori JA, Ferreira PM. Development of a high-speed 3-axis machine tool using a novel parallel-kinematics X–Y table,. International Journal of Machine Tools & Manufacture 2004;44(12–13):1355–71.
[14] Methods for performance evaluation of computer numerically controlled machine centers. ASME B5.54; 1992.
[15] Manipulating industrial robots—performance criteria and related test methods, ISO 9283; 1998.
[16] Elatta AY, Gen LP, Zhi FL, Daoyuan Y, Fei L. An overview of robotic calibration. Information Technology Journal 2004;3(1):74–8.
[17] Gong C, Yuan J, NI J. Nongeometric error identification and compensation for robotic system by inverse calibration. International Journal of Machine Tools and Manufacture 2000;40(14):2119–37.
[18] Zhuang H, Jiahua Y, Masory O. Calibration of Stewart platforms and other parallel manipulators by minimizing inverse kinematic residuals. Journal of Robotic Systems 1998;15(7):395–405.
[19] Chi-Haur W, Ho J, Young K. Design of robot accuracy compensator after calibration. IEEE Robotics and Automation Int 1988:780–5.
[20] Oliviers MP, Mayer JRR. Global kinematic calibration of a Stewart platform. Proceedings of the ASME Dynamic Systems and Control Division 1995;57:129–36.
[21] Masory O, Wang J, Zhuang H. Kinematic modeling and calibration of a Stewart platform. Advanced Robotics 1997;11:519–39.

[22] Gatla CS, Lumia R, Wood J, Starr G. An automated method to calibrate industrial robots using a virtual closed kinematic chain. IEEE Transactions on Robotics 2007;23(6):1105–16.
[23] Daney D. Étalonnage géométrique des robots parallèles. Doctoral thesis, Nice–Sophia Antipolis University, Nice, France; 2000.
[24] Ikits M, Hollerbach J. Kinematic calibration using a plane constraint. In: Proceedings of the IEEE international conference on robotics and automation, Albuquerque; 1997. p. 3191–6.
[25] Last P, Raatz A, Hesselbach J. Calibration of parallel kinematic structures—overview, classification and comparison. Robotic Systems for Handling and Assembly 2011;67:93–106.
[26] Verner M, Xi F, Mechefske C. Optimal calibration of parallel kinematic machines. Journal of Mechanical Design 2005;127(1):62–9.
[27] Motta STJM, De Carvalho GC, McMaster RS. Robot calibration using a 3D vision-based measurement system with a single camera. Robotics and Computer Integrated Manufacturing 2001;17(6):487–97.
[28] Watanabe A, Sakakibara S, Ban K, Yamada M, Shen G, Arai T. Kinematic calibration method for industrial robots using autonomous visual measurement. CIRP Annals—Manufacturing Technology 2006;55(1):1–6.
[29] Besnard S, Wisama K. Calibration of parallel robots using two inclinometers. In: Proceedings of the IEEE international conference on robotics and automation; 1999. p. 1758–63.
[30] Berg JO. Robot accuracy: a matter of programming. International Journal of Advanced Manufacturing Technology 1992;l7(4):193–7.
[31] Schroer K. RoboCal—the IPK robot calibration package. Industrial Robot: An International Journal 1994;21(6):35–9.
[32] Abtahi M, Pendar H, Alasty A, Vossoughi G. Experimental kinematic calibration of parallel manipulators using a relative position error measurement system. Robotics and Computer-Integrated Manufacturing 2010;26(6):799–804.
[33] Ota H, Shibukawa T, Uchiyama M, Forward kinematic calibration method for parallel mechanism using pose data measured by a double ball bar system. In: Proceedings of the Year 2000 parallel kinematic machines international conference, Ann Arbor, Michigan, USA; 2000. p. 57–62.
[34] Abderrahim M, Whittaker AR. Kinematic model identification of industrial manipulators. Robotics and Computer-Integrated Manufacturing 2000;16(1):1–8.
[35] Blaise J, Bonev IA, Monsarrat B, Briot S, Lambert JM, Perron C. Kinematic characterisation of hexapods for industry. Industrial Robot: An International Journal 2010;37(1):79–88.
[36] Renaud P, Andreff N, Martinet P, Gogu G. Kinematic calibration of parallel mechanisms: a novel approach using legs observation. IEEE Transactions on Robotics 2005;21(4).
[37] Gander W, Golub GH, Strebel R. Least-squares fitting of circles and ellipses. BIT Numerical Mathematics 1994;34(4):558–78.